Photochemistry and Vibrational Spectroscopy of the Trans and Cis Conformers of Acetic Acid in Solid Ar

E. M. S. Maçôas,[*,†,‡] **L. Khriachtchev,**[†] **R. Fausto,**[‡] **and M. Räsänen**[†]

Department of Chemistry, University of Helsinki, P.O. Box 55, FIN-00014 Helsinki, Finland, and Department of Chemistry (CQC), University of Coimbra, P-3004-535 Coimbra, Portugal

Acetic acid monomer has two stable geometries, the cis and trans conformers. The high-energy cis conformer has been recently detected experimentally for the first time [Maçôas et al. *J. Am. Chem. Soc.* **2003,** *125,* 16188]. The cis conformer can be produced in low-temperature rare-gas matrixes upon vibrational excitation of the ground-state trans conformer. Fast tunneling from *cis-* to *trans*-acetic acid takes place even at the lowest working temperatures (8 K), limiting the time available to study the high-energy form. Deuteration of the hydroxyl group reduces the tunneling rate by approximately 4 orders of magnitude, increasing accordingly the lifetime of the unstable conformer and its available concentration. In this work, we present a detailed analysis of the vibrational spectra of the cis form of four acetic acid isotopologues (CH_3COOH, CH_3COOD, CD_3COOH and CD_3COOD). Photolysis (193 nm) of the trans and cis forms of the perdeuterated compound was performed to evaluate the possible conformational dependence of photodissociation of acetic acid. However, no evidence of conformer specific photodissociation was found. The UV photolysis of the matrix-isolated acetic acid reveals very different products from the gas phase. Methanol complexed with carbon monoxide is the major product of photolysis of acetic acid isolated in Ar matrixes whereas it has never been observed as a photolysis product in the gas phase.

Introduction

Acetic acid has two planar conformers, trans and cis, with a computationally predicted energy difference of about 1883 cm^{-1} in favor of the trans conformer and an energy barrier for the trans to cis isomerization of 4432 cm^{-1}.[1] The spectroscopic properties and reactivity of the trans conformer have been studied in detail.[2−5] Nevertheless, despite the fact that acetic acid has been the subject of many experimental and theoretical studies,[1−10] including studies of conformational equilibrium in the gas phase and aqueous solution, only recently was the cis conformer detected experimentally.[11] The IR absorption spectra of *cis*-CH_3COOH was measured in an Ar matrix after excitation of the O−H stretching overtone of *trans*-CH_3COOH.[11] The preparation of cis acetic acid followed the method of selective IR pumping as was earlier applied.[12−14] The produced cis conformer tunnels back to the trans form in a minute time scale, which greatly limits the time available to study the high-energy conformer.[11] In that study, to overcome the limitation due to the lifetime of the unstable conformer, the IR absorption spectrum was collected during IR irradiation of *trans*-CH_3-COOH. Deuteration of the hydroxyl group slows down the tunneling rate, allowing a more accurate study of this species.

Small molecules with more than one conformer may exhibit conformer-selective photochemistry, as shown in the case of UV photolysis of formic acid (HCOOH) in solid argon.[15] Photochemical excitation, as opposed to thermal excitation, may deposit energy selectively into a molecule, thus inducing specific reaction channels.[16] Decomposition dynamics of acetic acid has been extensively investigated both theoretically and experimentally (see ref 17 for an overview on this subject and references therein). Theoretically, the ground-state decomposition channels of acetic acid were shown to depend on the initial conformational state,[18] the decarboxylation channel being associated with the cis conformer and the dehydration channel with the trans conformer. Experimentally, thermal decomposition in the gaseous phase occurs mainly via the decarboxylation and dehydration channels in a 1:2 proportion, yielding carbon dioxide with methane and ketene ($CH_2=C=O$) with water, respectively.[19,20] The gas-phase photodecomposition of acetic acid was shown to produce mainly acetyl and hydroxyl radicals.[21−24]

The present work has a 2-fold task. First, we study in detail the vibrational spectra of the cis conformer of acetic acid isolated in solid Ar, including three deuterated isotopologues (CH_3-COOD, CD_3COOH, and CD_3COOD), with special emphasis on the perdeuterated form. A revised vibrational assignment for the trans conformers is also proposed. Second, we study the photolysis of acetic acid isolated in Ar. Perdeuterated acetic acid was used to evaluate the conformational specificity of the 193 nm photodecomposition process. The lack of conformer dependent photodecomposition channels is discussed, as well as the influence of solid matrix on the photodecomposition products of acetic acid.[25−29] The 1:1 complex of methanol with carbon monoxide that is the major product of photolysis in the Ar matrix is identified on the basis of ab initio calculations.

Experimental and Computational Details

The gaseous samples were prepared by mixing acetic acid (Sigma-Aldrich, >99%) or its isotopologues (CD_3COOD and CH_3COOD, 99.5%), degassed by several freeze−pump−thaw

* To whom correspondence should be addressed. E-mail: emacoas@qui.uc.pt.
† University of Helsinki.
‡ University of Coimbra.

Spectroscopy of the Conformers of Acetic Acid in Ar

J. Phys. Chem. A, Vol. 108, No. 16, 2004 **3381**

cycles, with high-purity argon (AGA, 99.9999%), typically in the 1:2000 or 1:1000 proportions. The CD_3COOH species was obtained from the fully deuterated species by exchange of deuterium atom of the hydroxyl group with H_2O adsorbed on the inner surface of the sample container and the deposition line. The CD_3COOH isotopologue was also present in the CD_3COOD samples as an impurity. The gaseous mixtures were deposited onto a CsI substrate at 15 K in a closed cycle helium cryostat (APD, DE 202A) and subsequently cooled to 8 K. The IR absorption spectra ($7900-400$ cm^{-1}) were measured with a Nicolet SX-60 FTIR spectrometer. A liquid nitrogen cooled MCT detector and a Ge/KBr beam splitter were used to record the mid-IR absorption spectra, with spectral resolutions from 0.25 to 1.0 cm^{-1}, and a liquid-nitrogen-cooled InSb detector and a quartz beam splitter were used for the near-IR absorption spectra, with a spectral resolution of 0.5 cm^{-1}. Typically, $100-500$ interferograms were co-added.

Tunable pulsed IR radiation provided by an optical parametric oscillator (OPO Sunlite, Continuum, with IR extension) was used to produce *cis*-acetic acid via vibrational excitation of *trans*-acetic acid. [11] The pulse duration was ca. 5 ns, the spectral line width was ~0.1 cm^{-1}, and the repetition rate was 10 Hz. The pulse energy of the OPO in the $7000-5000$ cm^{-1} spectral region is ~0.5 mJ. The Burleigh WA-4500 wavemeter was used to control the OPO radiation frequency, providing an absolute accuracy better than 1 cm^{-1}. Whenever necessary, the IR absorption spectra were collected during pumping to compensate for the cis to trans tunneling process. The pumping beam was quasi-collinear with the spectrometer beam, and an interference filter transmitting in the $3300-1100$ cm^{-1} region was attached to the detector to prevent its exposure to the pumping radiation. The photodissociation was induced with 193 nm radiation of an excimer laser (MPB, MSX-250) operating at $1-3$ Hz with a typical pulse energy of 16 mJ. The UV irradiation of the trans conformer produces conversion to the cis conformer and vice versa. IR pumping of the UV-produced conformer was undertaken during UV irradiation to convert this conformer back into the conformer under study.

The ab initio calculations were performed using the GAUSSIAN98 package of programs. [30] The vibrational spectra of the cis and trans forms of various acetic acid isotopologues were calculated at the MP2/6-311++G(2d,2p) level. The ab initio Cartesian harmonic force constants obtained were later used in the normal coordinate analysis. The stable geometries, counterpoise-corrected interaction energies, and vibrational spectra of the complexes of methanol and carbon monoxide were evaluated at the same level of theory. [31]

Results and Discussion

Vibrational Assignment. For all studied isotopologues, acetic acid adopts exclusively the trans geometry in the as-deposited (nonirradiated) Ar matrix. To excite the acetic acid monomer at energies above the internal rotation barrier, we have used the overtone of the OH(D) stretching of the *trans*-conformer, observed at 6957.9, 6958.4, 5169.5, and 5167.8 cm^{-1} for CH_3COOH, CD_3COOH, CH_3COOD, and CD_3COOD, respectively. Excitation of this mode using a narrowband IR source promotes the conversion from the trans conformer to the cis form, as reported for a number of other carboxylic acids. [32] Figure 1 shows the spectrum obtained as a difference between the IR absorption spectra measured after and before the IR pumping of CH_3COOH and CD_3COOD. The bands pointing upward correspond to *cis*-acetic acid and the bands pointing downward correspond to the trans conformer. The spectral assignments
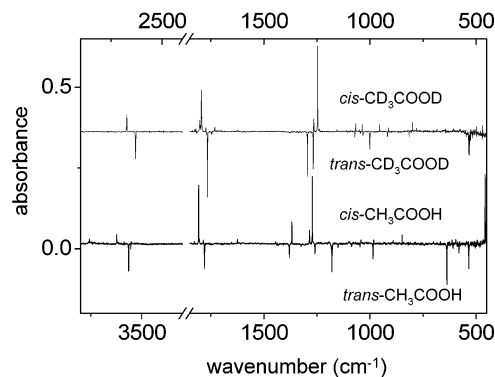
Figure 1. Difference IR absorption spectra showing the formation of *cis*-acetic acid (CH_3COOH and CD_3COOD) as a result of excitation of the $2\nu OH(D)$ modes of the trans conformer.

here presented are based on the calculated ab initio harmonic vibrational frequencies and normal coordinate analysis of acetic acid monomer. The experimental and calculated frequencies and normalized intensities as well as the potential energy distribution for the cis and trans conformers of CH_3COOH and CD_3COOD are presented in Tables 1 and 2. The data for CH_3COOD and CD_3COOH can be found in the Supporting Information (Tables S1 and S2).

Assignment for the Trans Conformer. In general, the PEDs calculated for the trans conformers agree with those reported earlier. [6] Several studies have been previously dedicated to the analysis of the IR absorption spectra of the *trans*-acetic acid in the gas phase and isolated in Ar matrixes. [2-5] In our work, we could not observe the $CH(D)_3$ stretching modes for any of the isotopologues studied, which agrees with their very low calculated intensity (see Tables 1 and 2). For the absorptions from 3600 to 1250 cm^{-1} (OH(D), $CH(D)_3$, C=O, and C−O stretches) our analysis supports the previous assignments. The discrepancy concerns the assignment of the COH bending mode (δ(COH)) made previously. [5] In that paper, an increase of the δ(COH) frequency upon deuteration was claimed. The δ(COH) modes of *trans*-CH_3COOH and *trans*-CD_3COOH were assigned to the bands at 1181 and 1208 cm^{-1}, respectively, whereas the δ(COD) modes for *trans*-CH_3COOD and *trans*-CD_3COOD were assigned to the bands at 1267 and 1268 cm^{-1}, respectively. We suggest a different assignment of the δ(COD) modes. On the basis of our calculations, the δ(COH) modes are close to 1200 cm^{-1} for *trans*-CH_3COOH and *trans*-CD_3COOH (assigned to the observed bands at 1179.8 and 1207.2 cm^{-1}, respectively), and for *trans*-CH_3COOD and *trans*-CD_3COOD the δ(COD) modes should be red shifted by more than 200 cm^{-1} from the δ(COH) bands. This is a normal red shift for the δ(COH(D)) mode, expected upon deuteration of the hydroxyl group. Therefore, in agreement with the theoretical predictions, we assign the bands observed at 955.4 and 1000.9 cm^{-1} to this vibration for *trans*-CH_3COOD and *trans*-CD_3COOD, respectively. These bands had been previously assigned to different $CH(D)_3$ deformation modes. [5] The comparison between observed and calculated intensities gives further support to the present revised assignment. For *trans*-CD_3COOD, the δ(COD) mode is expected to be located between the CD_3 bending modes (δ(CD_3)) and the CD_3 rocking modes (γ(CD_3)) and to have an intensity higher than all those vibrations (see Table 2). Accordingly, the band at 1000.9 cm^{-1} is located between the CD_3 angular deformation modes, being the highest intensity band in the 1100 to 800 cm^{-1} region. For *trans*-CH_3COOD, the δ(COD) had been assigned to a band at 1267 cm^{-1}, [5] which we reassign now to the ν(C−O) vibration. The ν(C−O) mode was previ-

TABLE 1: Observed Frequencies and Relative Intensities[a] of *cis*- and *trans*-CH₃COOH Isolated in an Ar Matrix at 8 K Compared with the Values Predicted at the MP2/6-311++G(2d,2p) Level[a]

assignment (PED)		ν_{calc}^{trans}	ν_{obs}^{trans}	assignment (PED)	ν_{calc}^{cis}	ν_{obs}^{cis}	$\Delta\nu_{calc}^{cis-trans}$	$\Delta\nu_{obs}^{cis-trans}$
ν(OH) (98)	a′	$3793.6^{(20.9)}$	$3563.8^{(42.4)}$	ν(OH) (99)	$3859.5^{(17.1)}$	$3622.6^{(8.4)}$	+65.9	+58.8
ν(HCH₂) s. (100)	a′	$3236.9^{(0.6)}$	3051^b	ν(HCH₂) s. (97)	$3229.7^{(0.5)}$		−7.2	
ν(HCH₂) as. (100)	a″	$3196.0^{(0.5)}$	2996^b	ν(HCH₂) as. (100)	$3178.0^{(0.9)}$		−18.0	
ν(CH₃) (98)	a′	$3115.3^{(0.3)}$	2944^b	ν(CH₃) (96)	$3099.4^{(0.9)}$		−15.9	
				δ(CH₃) + τ(C−O)^c		$1828.2^{(3.8)}$		
ν(C=O) (80)	a′	$1805.2^{(77.8)}$	$1779.0^{(91.0)}$	ν(C=O) (82)	$1832.6^{(66.3)}$	$1807.4^{(94.3)}$	+27.4	+28.4
						$1784.8^{(5.7)}$		
δ(HCH₂) as. (89)	a″	$1506.3^{(2.3)}$	$1438.8^{(1.8)}$	δ(HCH₂) as. (91)	$1514.3^{(2.1)}$	$1448.3^{(1.3)}$	+8.0	+9.5
δ(HCH₂) s. (90)	a′	$1501.0^{(4.3)}$	$1433.6^{(4.1)}$	δ(HCH₂) s. (92)	$1501.2^{(2.0)}$	$1444.5^{(2.7)}$	+0.2	+10.9
δ(CH₃) (82)	a′	$1434.5^{(14.1)}$	$1379.4^{(23.3)}$	δ(CH₃) (96)	$1421.5^{(12.8)}$	$1368.3^{(29.0)}$	−13.0	−11.1
			$1324.4^{(3.2)}$					
				ν(C−C) + τ(C−O)^c		FR$1285.4^{(21.2)}$		
ν(C−O) (25) + δ(COH) (29) + δ(CH₃) (19)	a′	$1352.7^{(10.4)}$	$1259.4^{(20.8)}$	ν(C−O) (24) + δ(COH) (32) + γ(CH₃) s. (18)	$1218.4^{(1.5)}$	$1192.9^{(3.0)}$	−134.3	−66.5
δ(COH) (47) + γ(CH₃) s. (16) + ν(C−O) (12)	a′	$1210.4^{(56.7)}$	$1179.8^{(82.0)}$	δ(COH) (55) + ν(C−O) (14) + ν(C−C) (12)	$1309.5^{(100.0)}$	FR$1271.9^{(100.0)}$	+99.1	+92.1
τ(C−O) + γ(C=O)^b			$1150.4^{(7.6)}$					
γ(CH₃) a. (70) + γ(C=O) (21)	a′	$1084.6^{(1.4)}$	$1047.2^{(5.5)}$	γ(CH₃) a. (70) + γC=O (20)	$1078.7^{(0.9)}$	$1042.4^{(6.5)}$	−5.9	−4.8
γ(CH₃) s. (61) + ν(C−O) (20)	a″	$1011.7^{(21.4)}$	$985.5^{(24.7)}$	γ(CH₃) s. (61) + ν(C−O) (20)	$1002.9^{(2.9)}$	$982.2^{(5.3)}$	−8.8	−3.3
				2τ(C−O)^c		$890.5^{(4.1)}$		
ν(C−C) (58) + ν(C−O) (37)	a′	$871.8^{(2.1)}$		ν(C−C) (53) + ν(C−O) (38)	$864.9^{(10.8)}$	$848.6^{(8.0)}$		
τ(C−O) (77) + γ(C=O) (15)	a″	$663.4^{(23.9)}$	$637.8^{(74.7)}$	τ(C−O) (79) + γ(C=O) (20)	$468.2^{(27.2)}$	$458.0^{(95.9)}$	−195.2	−179.8
δ(OCO) (85)	a′	$586.3^{(9.7)}$	$580.4^{(16.0)}$	δ(OCO) (86) + ν(C−C) (11)	$600.7^{(2.0)}$		+14.4	
γ(C=O) (69) + τ(C−O) (23) + γ(CH₃) a. (15)	a″	$553.1^{(8.5)}$	$534.2^{(38.5)}$	γ(C=O) (63) + τ(C−O) (19) + γ(CH₃) a. (18)	$605.2^{(0.4)}$		+52.1	
δ(CC=O) (86)	a′	$427.0^{(1.1)}$	428^b	δ(CC=O) (84) + γ(CH₃) s. (10)	$436.0^{(1.0)}$		+9.0	
τ(CH₃) (97)	a″	$80.2^{(0.06)}$		τ(CH₃) (98)	$95.2^{(0.3)}$		+15	

[a] The observed and calculated intensities were normalized by the intensity of the strongest band of both cis and trans conformers. The normalized values are shown in parentheses. The calculated potential energy distributions on the basis of the ab initio harmonic force constant are also shown. [b] From ref 5. [c] Tentative assignment. Symbols: ν- stretching; δ- bending; γ- rocking; τ-torsion; FR− involved in Fermi resonance.

ously assigned to a band at 1271 cm⁻¹ that is very weak in our spectra and it is most probably due to matrix site effects.[5] On the other hand, for *trans*-CD₃COOD, the ν(C−O) and δ(COD) modes were previously assigned to the bands at 1296 and 1268 cm⁻¹,[5] and they are observed in our spectra at 1294.5 and 1267.5 cm⁻¹, respectively. Those are strong bands probably caused by coupling of ν(C−O) with a non fundamental mode (see Table 2).

Another discrepancy with the assignments made in ref 5 concerns the COH torsion (τ(C−O)) and C=O rocking modes (γ(C=O) in this work and simply γ in ref 5) of *trans*-CH₃COOH and -CD₃COOH. These two A″ modes are expected in the 700−500 cm⁻¹ region. In the present work, the τ(C−O) modes are assigned to the higher frequency and stronger bands observed in this region (637.8 and 609.0 cm⁻¹ for CH₃COOH and CD₃COOH, respectively) (see Table 1). This mode is also observed above 600 cm⁻¹ (at 635.4 cm⁻¹) for *trans*-formic acid in solid Ar.[13,14] The γ(C=O) mode of CH₃COOH is here assigned to the band observed at lower frequencies (534.2 cm⁻¹). For CD₃COOH, this mode was not observed due to its low intensity but we believe it should be assigned to the band at 479 cm⁻¹ reported previously.[5] Our assignment for the τ(C−O) and γ(C=O) modes is in the reverse order with respect to the literature data.[1,2,5] The present assignment is based on our ab initio calculations, and it respects the predicted relative position and intensities of the bands originated by the 3 modes absorbing in the 700−500 cm⁻¹ region (see Table 1), and it is also supported by previously reported results on normal coordinate analysis.[6]

Assignment for the Cis Conformer. The spectral assignment for the cis conformers is quite straightforward based on the ab initio spectra. The ν(OH(D)) mode of *cis*-acetic acid is blue shifted by 40−60 cm⁻¹ from the corresponding mode of the trans conformers, in good agreement with the ab initio predic-

tions for acetic acid and also with the observed analogous shift of formic acid (≈60 cm⁻¹).[13,14] The ν(C=O) mode appears also 20−30 cm⁻¹ shifted to higher wavenumbers in the cis conformers as compared with the trans conformers (see Tables 1 and 2). The methyl stretching modes, predicted with very low intensities in the 3300−3000 cm⁻¹ and 2400−2200 cm⁻¹ spectral regions for CH₃COOH and CD₃COOD, respectively, were not observed experimentally.

For CH₃COOH, the ν(C−O) and δ(COH) vibrations are strongly coupled and perhaps they can be better defined as the COH−CO deformation modes, similarly to formic acid.[13,14] According to the calculations, the mode with the highest contribution from the δ(COH) coordinate of *cis*-CH₃COOH (1309.5 cm⁻¹) is blue shifted by almost 100 cm⁻¹ from the corresponding mode of the trans conformer (1210.4 cm⁻¹). In contrast, for *cis*-CH₃COOH a mode with nearly the same contribution from the ν(C−O) and δ(COH) coordinates (1218.4 cm⁻¹) is predicted to be red shifted by more than 100 cm⁻¹ from the corresponding mode of trans (1352.7 cm⁻¹). For both conformers, the δ(COH) mode is predicted to be the most intense vibration in the 1400−1200 cm⁻¹ region. For *cis*-CD₃-COOD, the ν(C−O) and δ(COD) modes are not coupled significantly and the assignments presented in Table 2 agree with both the computational band positions and intensities.

The C−C stretching modes (ν(C−C)) are observed for the cis conformers in the 850−800 cm⁻¹ region. These modes are predicted to be much more intense in the cis form than in the trans conformer. Below 800 cm⁻¹ our analysis is limited by the relatively low concentration of the cis form. Therefore, we could only detect strong modes for *cis*-CH₃COOH like the τ(C−O) fundamental. This mode absorbs at 458.0 cm⁻¹, red shifted by 180 cm⁻¹ from the corresponding band of *trans*-CH₃COOH, which agrees with the 195 cm⁻¹ shift predicted by the ab initio calculations. A band observed at 890.5 cm⁻¹ is

TABLE 2: Observed Frequencies and Relative Intensities[a] of *cis*- and *trans*-CD_3COOD Isolated in an Ar Matrix at 8 K Compared with the Values Predicted at the MP2/6-311++G(2d,2p) Level

assignment (PED)		ν_{calc}^{trans}	ν_{obs}^{trans}	assignment (PED)	ν_{calc}^{cis}	ν_{obs}^{cis}	$\Delta\nu_{calc}^{cis-trans}$	$\Delta\nu_{obs}^{cis-trans}$
ν(OD) (99)	A′	$2759.3^{(16.1)}$	$2630.4^{(27.7)}$ $2629^{(26.5)}$	ν(OD) (99)	$2809.9^{(13.4)}$	$2675.5^{(9.4)}$ $2672.9^{(21.2)}$	+50.6	+42.5
$\nu(DCD_2)$ s. (99)	A′	$2401.2^{(0.4)}$	2275^b	$\nu(DCD_2)$ s. (98)	$2394.1^{(0.2)}$		−7.1	
$\nu(DCD_2)$ as. (100)	A″	$2365.2^{(0.3)}$	2240^b	$\nu(DCD_2)$ as. (100)	$2352.5^{(0.6)}$		−12.7	
$\nu(CD_3)$ (98)	A′	$2239.2^{(<0.1)}$	2116^b	$\nu(CD_3)$ (98)	$2228.4^{(0.3)}$		−10.8	
ν(C=O) (85)	A′	$1792.1^{(94.0)}$	$1769.8^{(6.4)}$ $1765.0^{(80.7)}$ $1746.8^{(4.5)}$ $1743.7^{(3.5)}$ $1376.4^{(2.4)}$	ν(C=O) (86)	$1821.6^{(89.4)}$	$1863.8^{(3.2)}$ $1801^{(31.9)}$ $1794.4^{(96.4)}$ $1730.3^{(6.1)}$	+29.5	+29.4
ν(C−O) (43) + ν(C−C) (31)	A′	$1319.2^{(75.9)}$	$^{FR}1294.5^{(54.4)}$ $^{FR}1267.5^{(49.2)}$	ν(C−O) (39) + ν(C−C) (30) + δ(CD) (10)	$1280.5^{(100.0)}$	$1367.7^{(1.9)}$ $^{FR}1264.6^{(15.6)}$ $^{FR}1246.2^{(100.0)}$ $1238.1^{(5.7)}$	−38.7	−34.8
$\delta(CD_3)$ (63) + $\delta(DCD_2)$ s. (16) + ν(C−O) (14)	A′	$1106.1^{(4.4)}$	$1071.3^{(8.2)}$	$\delta(CD_3)$ (61) + $\delta(DCD_2)$ s. (20) + ν(C−O) (11)	$1100.6^{(8.1)}$	$1066.9^{(8.5)}$	−5.5	−4.4
$\delta(DCD_2)$ a. (91)	A″	$1084.9^{(1.1)}$	$1044.8^{(1.8)}$	$\delta(DCD_2)$ a. (94)	$1090.2^{(1.1)}$	$1050.5^{(2.3)}$	+5.3	+5.7
$\delta(DCD_2)$ s. (81) + $\delta(CD_3)$ (15)	A′	$1072.4^{(6.3)}$	$1033.2^{(4.9)}$	$\delta(DCD_2)$ s. (78) + $\delta(CD_3)$ (18)	$1073.4^{(8.8)}$	$1036.5^{(9.7)}$	+1.0	+3.3
δ(COD) (62) + δ(OCO) (12)	A′	$1019.1^{(22.7)}$	$1000.9^{(22.1)}$	δ(COD) (58) + $\gamma(CD_3)$ s. (14)	$973.5^{(5.9)}$	$954.6^{(5.7)}$	−45.6	−56.3
$\gamma(CD_3)$ a. (51) + γ(C=O) (42)	A″	$940.7^{(2.2)}$	$917.9^{(8.6)}$	$\gamma(CD_3)$ a. (52) + γ(C=O) (40)	$933.3^{(1.4)}$	$913.1^{(4.4)}$	−7.4	−4.8
$\gamma(CD_3)$ s. (65) + ν(C−O) (22)	A′	$832.8^{(8.4)}$	$815.7^{(6.4)}$	$\gamma(CD_3)$ s. (40) + δ(COD) (23) + ν(C−C) (23)	$795.2^{(1.7)}$		−37.6	
ν(C−C) (54) + δ(COD) (18) + ν(C−O) (14) + $\delta(CD_3)$ (11)	A′	$768.5^{(0.9)}$		ν(C−C) (27) + ν(C−O) (40) + $\gamma(CD_3)$ s. (17)	$813.8^{(9.1)}$	$799.3^{(9.4)}$	−19.0	
γ(C=O) (28) + $\gamma(CD_3)$ a. (32) + τ(C−O) (41)	A″	$550.6^{(9.7)}$	$534.7^{(27.0)}$	γ(C=O) (55) + $\gamma(CD_3)$ a. (39)	$516.4^{(2.1)}$		−34.2	
δ(OCO) (75) + δ(COD) (13)	A′	$536.4^{(12.4)}$	$530.3^{(24.5)}$	δ(OCO) (76) + ν(C−C) (14)	$565.3^{(0.2)}$		+28.2	
τ(C−O) (58) + γ(C=O) (34)	A″	$421.7^{(12.1)}$		τ(C−O) (89) + γ(C=O) (10)	$352.0^{(1.5)}$		−69.7	
δ(CC=O) (76) + $\gamma(CD_3)$ s. (18)	A′	$375.5^{(1.0)}$		δ(CC=O) (75) + $\gamma(CD_3)$ s. (18)	$377.7^{(17.3)}$	$382.3^{(50.6)}$	+2.2	
$\tau(CD_3)$ (97)	A″	$58.9^{(<0.1)}$		$\tau(CD_3)$ (98)	$69.2^{(0.5)}$		+10.3	

[a] The observed and calculated intensities were normalized by the intensity of the strongest band of both cis and trans conformers. The normalized values are shown in parentheses. The calculated potential energy distributions on the basis of the ab initio harmonic force constant are also shown. [b] From ref 5. Symbols: ν, stretching; δ, bending; γ, rocking; τ, torsion; FR, involved in Fermi resonance.

tentatively assigned to the C−O torsion overtone of *cis*-CH_3COOH. In this case, the anharmonicity of the τ(C−O) mode in *cis*-CH_3COOH is similar to that of the analogous mode of *cis*-HCOOH ($\approx$13 cm^{-1}).[13]

Several low-intensity bands are unassigned in Tables 1 and 2 or assigned tentatively to overtones or combination modes. Some of them can also be due to matrix-site effects. It is not our purpose to discuss the assignment of those bands. It should be mentioned only that the spectrum of *cis*-CH_3COOH shows a relatively intense band at 1285.4 cm^{-1} that probably originates from a nonfundamental mode with enhanced intensity due to coupling with the very intense δ(COH) mode (at 1271.9 cm^{-1}). It is assigned tentatively to the ν(C−C) + τ(C−O) combination mode. In the case of CD_3COOD, both conformers exhibit a doublet in the region of the ν(C−O) mode separated by 18 and 27 cm^{-1} for cis and trans, respectively. We believe that this is due to the coupling of the νC−O mode with a nonfundamental mode rather than due to matrix site effects.

193 nm Photolysis. One of the motivations of this work was to investigate the possible conformational selectivity of UV photolysis of acetic acid. In an Ar matrix, conversion of *cis*-CH_3COOH and *cis*-CD_3COOH to the corresponding trans forms by tunneling is very fast, which limits the concentration of the cis conformer. Therefore, the influence of the molecular conformation on the photolysis of acetic acid is better studied for the CD_3COOD isotopologue, due to its relatively slow cis-to-trans tunneling. Indeed, for this deuterated molecule, the half-life of the cis conformer is approximately 5 days, whereas for *cis*-CH_3COOH it is 16 s.[11] As already mentioned, the cis conformer appears as one of the products of UV photolysis of
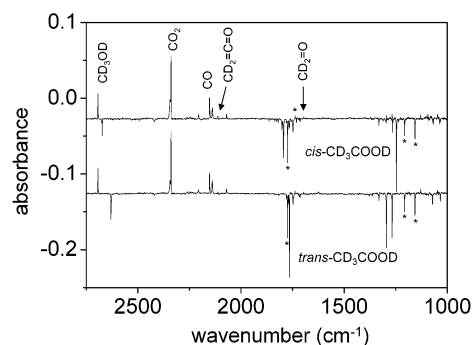
Figure 2. Difference IR absorption spectra showing the result of 193 nm photolysis of the cis and trans conformers of perdeuterated acetic acid in solid Ar at 8 K. Bands marked with an asterisk are from CD_3COOH present as an impurity in the sample.

trans-CD_3COOD, and vice versa. Thus, to minimize the effect of UV-induced rotamerization, UV photolysis of one conformer (trans or cis) was undertaken while the other conformer was pumped with resonant IR radiation. Excitation of the OD stretching overtone of the conformer produced by UV radiation converts it back to the starting conformer. The ν(OD) overtone is observed at 5167.8 and 5257.4 cm^{-1} for *trans*- and *cis*-CD_3COOD isolated in solid Ar.

The main photolysis products are molecular complexes involving CO_2 or CO, namely CO complexed with methanol (see later). No conformational dependence was found upon photolysis of CD_3COOD, as seen in Figure 2. We can suggest a number of possible reasons why the acetic acid photolysis is conformationally independent, in contrast to the photolysis of

formic acid. If vibrational relaxation in the excited electronic state of acetic acid is faster than dissociation, as was suggested for excitation at 218 and 200 nm,[22,23] then photodecomposition is expected to be a conformationally independent process. In formic acid, torsional randomization was assumed to be a slower process as compared to formation of the transition state for decomposition.[15] In fact, it has been estimated recently that in the S_1 surface isomerization of formic acid occurs on a picosecond time scale, whereas decomposition takes place in a femtosecond time scale.[33] In matrix-isolated formic acid, the S_1 Franck−Condon geometry relaxes to a vibrationally excited ground state and decomposition results mainly in formation of molecular products.[15] The same process was used to explain molecular elimination upon photolysis of formic acid in the gas phase.[34] In contrast, it is known that the primary gas-phase photolysis products of acetic acid are mainly radicals (CH_3CO, OH, CH_3, COOH),[22−24,35] even though molecular elimination products upon UV broadband photolysis were reported in earlier works.[36] This indicates that the decomposition takes place mainly on the excited-state surfaces rather than in the vibrationally excited ground state. The molecular products of solid-state photolysis of acetic acid, formed upon cage-induced recombination of the primary radicals, indicate that the branching ratio for radical formation is conformationally independent. The photodecomposition dynamics in acetic acid has been studied theoretically using the MP2 and CASSCF methods.[17] In that study, it has been shown that the transition state for C−C cleavage on the T_1 surface has a geometry very similar to that of *cis*-acetic acid, whereas the transition state for C−O cleavage on the T_1 surface and for both C−C and C−O cleavages on the S_1 surface are connected geometrically to *trans*-acetic acid.[17] This means that the branching ratio between radicals could in principle be affected by the molecular conformation. In practice, because $T_1 \leftarrow S_0$ is a forbidden transition and at the S_1/T_1 crossing point the T_1 Franck−Condon geometry is already relaxed to a geometry bearing no memory of the initially excited conformer, decomposition to radicals on the T_1 surface seems to be conformationally independent. On the S_1 surface, the C−O cleavage is the only energetically accessible process. Finally the UV-induced isomerization competes with photodecomposition upon 193 nm irradiation of acetic acid, as seen from the production of *cis*-CD_3COOD upon irradiation of *trans*-CD_3-COOD, and vice versa. This might be another reason for photodecomposition to be a conformationally independent process in acetic acid as opposed to formic acid, where isomerization does not compete appreciably with decomposition.

The easily identified photodecomposition products of CD_3-COOD are methanol,[37] carbon monoxide, and carbon dioxide.[38−40] In addition, we could detect also weaker bands from formaldehyde and ketene.[41,42] These species are isolated as complexes with the corresponding photolysis product, as will be later discussed. The same products are observed upon photolysis of CH_3COOH, with some small differences in the branching ratios as compared with the deuterated isotopologue. Figure 3 is a difference spectrum showing the result of photolysis of CH_3-COOH in solid Ar. In Table 3 the emerging bands upon photolysis of CD_3COOD and CH_3COOH are listed together with previously reported data on the relevant monomeric species isolated in Ar.

Most interestingly, this is the first time that methanol and carbon monoxide are among the products of molecular elimination channels upon photolysis of monomeric acetic acid. These products might be the result of recombination of acetyl and hydroxyl radicals formed on the S_1 or T_1 surfaces,[17] which
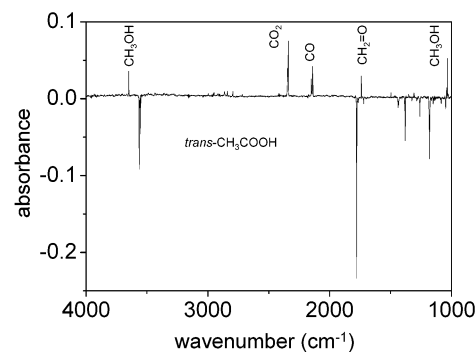
Figure 3. Difference IR absorption spectrum showing the result of 193 nm photolysis of *trans*-CH_3COOH isolated in solid Ar at 8 K.

remain in close contact within the same matrix cage after decomposition of acetic acid. Methanol and carbon monoxide could also be formed upon further photolysis of primary acetic acid decomposition products, for instance, photolysis of ketene in the presence of water.[43] Figure 4 illustrates a possible photodecomposition scheme. According to this scheme, the final products are dictated by the recombination of radicals, which is caused by the matrix-cage effect.[29] The matrix cage is known to affect substantially the decomposition dynamics of the isolated molecule due to the fact that, even for the light fragments, cage exit is a rather improbable phenomenon. Furthermore, because the molecular species formed as a result of permanent dissociation remain in the same cage, they might form stable complexes. In fact, photolysis of matrix isolated species has been used to prepare various 1:1 molecular complexes.[44−49]

Another product of photolysis of acetic acid is CO_2. On the basis of the frequently used ratio of ∼10 between CO_2 and CO absorption cross sections,[50,51] the CO/CO_2 product ratio upon photolysis is ∼5. Methane is expected to be formed together with CO_2, from recombination of the $CH(D)_3$ and $OCOH(D)$ radicals formed after C−C bond cleavage on the T1 surface.[17] Nevertheless, the bands of methane are not readily identified after photolysis of CD_3COOD (Table 3), which is most probably due to the much smaller IR absorption cross section of methane modes as compared with CO_2. In the photolysis of CH_3COOH we assigned one band emerging at 1308.3 cm^{-1} to methane reported previously at 1307.7 cm^{-1}.[52] The C−H stretching mode of the methane monomer is known to be a broad band in rare-gas matrixes.[52] This can explain why this mode is not observed upon photodissociation of CH_3COOH despite having a higher intrinsic intensity than the bending mode.[53]

A band at 2112.1 cm^{-1}, rising upon photolysis of CD_3COOD, is assigned to the ν(C=O) mode of deuterated ketene (CD_2=C=O). In agreement, this mode is observed for CH_2=C=O in the 2134−2144 cm^{-1} region and it is predicted by ab initio calculations to shift toward lower frequencies by 21.6 cm^{-1} for CD_2=C=O.[42] It is the strongest mode of ketene,[42] with an absorption cross section much larger than any other vibration of this species (∼555 and 440 km/mol, calculated for CH_2=C=O and CD_2=C=O, respectively). The 2112.1 cm^{-1} band increases quickly in the earlier stages of photolysis and decreases upon long photolysis. This behavior is in agreement with the fact that ketene can also be photolyzed with 193-nm radiation.[43] The estimated CO:CD_2=C=O ratio is ∼20:1, even in the earlier stages of photolysis. This means that the photolysis channel leading to production of ketene is minor or its formation rate is comparable with its decomposition in the present experimental conditions. Ketene is not readily identified as a product of photolysis of CH_3COOH because the ν(C=O) band of CH_2=C=O overlaps with the absorption of carbon monoxide.

Spectroscopy of the Conformers of Acetic Acid in Ar

J. Phys. Chem. A, Vol. 108, No. 16, 2004 **3385**

TABLE 3: Comparison between the Observed IR Frequencies (cm⁻¹) for the 193 nm Photolysis Products of CD₃COOD and CH₃COOH with Reported Data on Monomeric CD₃OD/CH₃OH, CD₄/CH₄, CO₂, CO, CD₂=O/CH₂=O, and CH₂=C=O Isolated in Solid Ar[a]

| CD₃COOD products		lit. data[b]		mode	lit. data[b]		CH₃COOH products	
		CD₃OD			CH₃OH			
2693.6	m	2706.1	m	ν(OH)	3667.3	s	3649.6	m
2205.9	w	2219.1	w	ν(CH₃)	3005.3	m	2996.8	vw
2258	vw	2254.3	m	ν(CH₃)	2961.9	s	2949.2	vw
2246	vw							
2070	w	2078.3	m	ν(CH₃)	2847.9	s	2839.5	vw
		1031.3	m	δ(CH₃)	1474.1	vw		
		1068.1	vw	δ(CH₃)	1465.8	vw		
1129	w	1132.7	m	δ(CH₃)	1451.4	vw		
782.4	w	775.4	m	δ(COH)	1335	m	1351	vw
858.1	vw	860.4	vw	ρ(CH₃)	1157	vw		
		1055.2	vw	ρ(CH₃)	1076.7	vw		
978.8	w	983.4	m	ν(CO)	1034.0	vs	1034	s
				τ(CO)	240	vs		
		CD₄[c]			CH₄			
		2260.3	w	ν(CH₃)	3037.0	s		
		993.4	w	δ(CH₃)	1307.7	s	1308.3	w
		CO₂[d]						
2347.5	br	2345.2	vs	ν(CO₂)			2345.6	br
2344.5	br						2344.4	br
2341.6	br						2340.2	s
2339.2	vs	2339.0	vs	ν(CO₂)			2338.9	vs
663.9	m	663.3	m	δ(CO₂)			663.9	m
662.3	m	661.8	m	δ(CO₂)			662.3	m
		CO[e]						
2152.5	m						2152.0	m
2151.9	m						2151.6	m
2151.5	sh						2151.0	sh
2150.3	m						2149.9	m
							2141.1	sh
2140.0	m	2140.1	sh	ν(C≡O)ᴰ			2140.2	m
2139.3	m	2138.5	s	ν(C≡O)ᴹ			2140.0	m
		2136.7	sh	ν(C≡O)ᴹ			2139.4	sh
2138	br						2138.3	m
		CD₂=O			CH₂=O			
		2176.8	s	ν(CH₂)	2863.0	s	2863	vw
		2069.1	s	ν(CH₂)	2797.1	s	2794.2	w
1696.1	vw	1697.8	s	ν(C=O)	1742.0	s	1739.9	m
		1099.1	vw	δ(CH₂)	1498.8	m	1496.7	w
		987.1	w	ρ(CH₂)	1244.8	w		
		938.3	vw	ω(CH₂)	1168.0	w		
				CH₂=C=O				
				ν(CH₂)	3062	m		
2112.1	w			ν(C=O)	2140	vs	2140[f]	m
				δ(CH₂)	974	m		
				ρ(C=O)	579	m		
				ρ(C=O)	525	s		

[a] Symbols: vs, very strong; s, strong; m, medium; w, weak; vw, very weak; br, broad; sh, shoulder; ν, stretching; δ, bending; ρ, rocking; ω, wagging and τ, torsion. [b] Data were taken from refs 37–42 and 52. [c] Data of CD₄ isolated in Kr matrixes taken from ref 52. [d] The splitting of the CO₂ bands was assigned to molecules isolated in different sites in ref 40. [e] The letters M and D stand for monomer and dimer, respectively.[38,39] [f] Band overlapping with the envelope of bands from CO, see text for a detailed explanation.

Nevertheless, it can be seen in Figure 5 that the band shape of the carbon monoxide absorption near 2140 cm⁻¹ changes significantly during photolysis, and the overlapping ketene band can cause this modification. Furthermore, after 600 pulses there is a band at 1593.9 cm⁻¹ that can be due to formation of complexed water, which is the other molecular species produced together with ketene.[15] This band disappears after 3300 pulses, which probably indicates that water reacts with the photolysis products of ketene. The major products of 193 nm photolysis of ketene are CH₂ + CO and HC≡CO + H in a 1:3 proportion.[15] Because these radicals will be in close contact with water inside

the matrix cage, they can react with water, forming various radicals, which react further producing at some point stable molecular species (formaldehyde, carbon monoxide, and molecular hydrogen; see Figure 4). Notice that formaldehyde (CH₂=O) might also be generated from photolysis of the methanol molecules formed directly from recombination of the acetyl and hydroxyl radicals (Figure 4).[54] The formation of formaldehyde from photolysis of CH₃COOH is evident because we have detected the four strongest vibrations of this molecule (see Table 3). However, only the νC=O band of deuterated formaldehyde was observed (1696.1 cm⁻¹) upon photolysis of
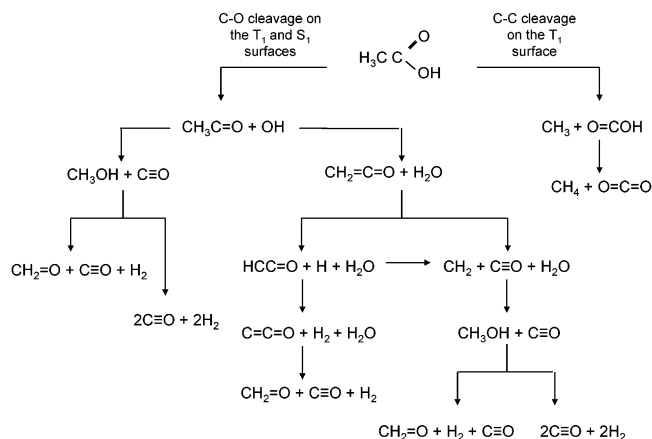
Figure 4. Photodecompositiom channels of acetic acid. In addition to the presented decomposition channels, there is also a possibility of recombination of the primary radicals back to acetic acid in the vibrationally excited ground state that can dissociate directly into the observed molecular products of thermal decomposition (CH_2=C=O + H_2O and CH_4 + CO_2).
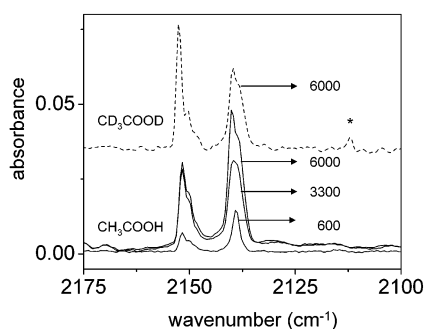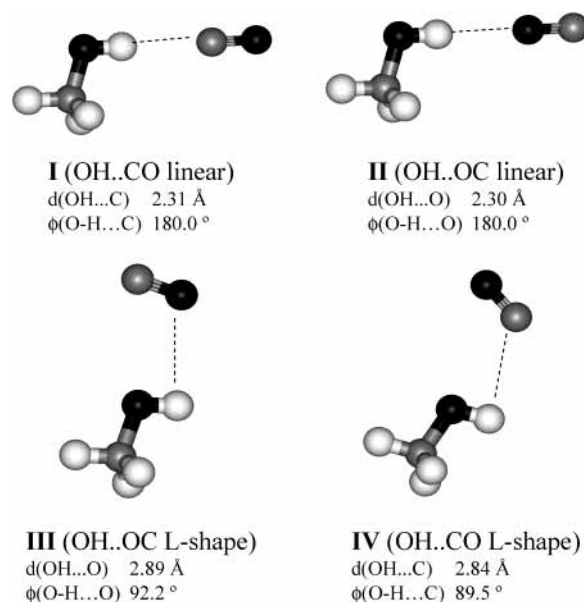

Figure 5. IR absorption bands emerging in the 2175−2100 cm^{-1} region upon 193 nm photolysis of CH_3COOH with 600, 3300, and 6000 pulses. The same region is shown for photolysis of CD_3COOD (- - -) after 6000 pulses of 193 nm radiation for comparison. The band marked with an asterisk was assigned to deuterated ketene (CD_2=C=O).

CD_3COOD. This emerging band is very weak, indicating that formaldehyde is a minor product of photolysis of CD_3COOD.

Complex between Carbon Monoxide and Methanol. Methanol formed upon 193 nm photolysis of acetic acid in solid Ar is produced together with carbon monoxide in the same matrix cage. It is known that when methanol is isolated in an Ar matrix doped with 2% of carbon monoxide a 1:1 complex is formed between the two molecules.[55] On one hand, the bands of methanol are consistent with the formation of one specific type of complex (see discussion later). On the other hand, carbon monoxide can be produced upon solid-state photolysis of acetic acid via various mechanisms, such as photolysis of ketene in the presence of water, photolysis of methanol, and direct recombination of acetyl and hydroxyl radical. From the possible decomposition pathways shown in Figure 4, carbon monoxide could be sharing the matrix cage with methanol, formaldehyde, and molecular hydrogen or with another carbon monoxide molecule and hydrogen. In fact, the produced carbon monoxide upon UV irradiation of acetic acid exhibits two sets of bands separated by ∼10 cm^{-1}, indicating that at least two different types of complexes with CO are produced.

Previously, a red shift (18 cm^{-1}) was observed for the ν-(OH) mode of CH_3OH isolated in an Ar matrix containing 2% of CO.[55] This shift agrees with our data on ν(OH) of CH_3OH formed upon photolysis of CH_3COOH (Table 3). A proportional shift was observed in the ν(OD) mode of CD_3OD complexed with CO (13 cm^{-1}) as compared with the monomer isolated in

I (OH..CO linear)
d(OH...C) 2.31 Å
φ(O-H...C) 180.0 °

II (OH..OC linear)
d(OH...O) 2.30 Å
φ(O-H...O) 180.0 °

III (OH..OC L-shape)
d(OH...O) 2.89 Å
φ(O-H...O) 92.2 °

IV (OH..CO L-shape)
d(OH...C) 2.84 Å
φ(O-H...C) 89.5 °

Figure 6. Optimized geometries for the 1:1 complex between methanol and carbon monoxide. Relevant geometrical parameters of complexes are shown.

TABLE 4: Comparison between Predicted [MP2/6-311++(2d,2p)] Frequency Shifts for the Four Stable Structures of the Complex between Methanol and Carbon Monoxide with Respect to the Free Monomers and the Observed Shifts for the Complex Isolated in Solid Ar

free monomer (cm^{-1})	I OH⋯CO linear	II OH⋯OC linear	III OH⋯OC L-shape	IV OH⋯CO L-shape	obsd[a]
3902.9	−26.8	+12.0	−7.4	−9.1	−17.7
3205.0	−7.5	−2.2	+1.1	−0.7	−8.5
3144.2	−11.0	−4.4	+1.8	+1.5	−12.7
3075.1	−8.1	−3.4	+1.0	+0.7	−8.4
2120.1	+12.5	−3.3	−1.6	+4.3	+12
1544.8	+0.3	+0.2	−0.1	−0.2	
1532.1	+0.2	+0.2	−0.5	−0.7	
1508.1	−0.9	−0.3	−0.4	−0.7	
1387.3	+31.8	+12.2	−0.4	−1.4	+16.3
1191.2	+0.2	0.0	+0.3	−0.2	
1095.4	+19.0	+7.3	0.0	+5.1	
1053.9	+9.8	+3.5	−0.1	+0.2	−0.3
288.3	+195.1	+76.9	+9.8	+29.3	
E_{int}[b]	−1.66 (−1.24)	−0.60 (−0.48)	−0.72 (−0.53)	−1.06 (−0.56)	

[a] Observed shifts with respect to the bands of the free monomers isolated in an Ar matrix.[37] [b] BSSE corrected interaction energy (kJ mol^{-1}) calculated at the at the MP2/6-311++(2d,2p) level and values taken form ref 56 in parentheses.

solid Ar.[37] The red shift of the ν(OH) frequency of methanol upon complexation with CO disagrees with the earlier computationally predicted blue shift for all stable geometries of this complex.[56] In view of this disagreement, we performed geometry optimizations and energy calculations based on those geometries with a more complete basis set. In Figure 6 the four stable geometries of the complex formed between CH_3OH and CO are shown. The energetics of these structures and the expected frequency shifts for the complexed units with respect to the free monomers appear in Table 4.

From the four optimized geometries of the complex, two have a linear arrangement of the CO molecule with respect with the OH bond (I and II) and two have an L-shape arrangement (III and IV). Structure I has the OH⋯CO interaction whereas structure II has an interaction of the OH⋯OC type. Both of

them are predicted to have the OH···O/C distances and O−H···O/C angles characteristic of interactions via hydrogen bonds (2.3 Å and 180°), as shown in Figure 6. In structure III the oxygen atom of CO is closer to the hydrogen atom of the hydroxyl group in methanol, whereas in structure IV it is the carbon atom of CO that is closer to the hydroxylic hydrogen. For III and IV, the OH···O and OH···C calculated distances are 2.9 and 2.8 Å, respectively, and the O−H···O/C angles deviate from the characteristic values of hydrogen bonded systems. The energies of the stable geometries of the 1:1 complex between methanol and CO are in qualitative agreement with the previously reported data.[56] The only difference is the somewhat increased stability of structure IV with respect to the other structures. Our calculations predict a complexation-induced red shift in the ν(OH) mode of methanol for structures I, III, and IV and a blue shift for complex II.

The formation of complex II in the matrix can be ruled out because the predicted complexation shift of the ν(OH) is positive (blue) whereas the observed shift is negative (red). Among the three structures exhibiting a complexation-induced red shift in the ν(OH) mode, complex I exhibits vibrations in good agreement with the experiment, and it has the highest interaction energy. This is particularly evident for ν(OH), the three ν(CH), and the δ(COH) modes (observed shifts of −26.8, −7.5, −11.0, −8.1, and +31.8 and the corresponding predicted values −17.7, −8.5, −12.7, −8.4, and +16.3). For the most stable complex structure, calculations predict a blue shift of 12.5 cm^{-1} on the νC≡O vibration, in good agreement with the observed shift of about +12 cm^{-1} for the high-frequency set of bands of CO. Thus, according to the calculations, the high-frequency set of bands of CO ($\sim$2150 cm^{-1}) should be assigned to complex I. The identification of complex I is further supported by the fact that the predicted effect of deuteration on the complexation induced shift (a 7 cm^{-1} smaller red shift for νOD) agrees with the observed isotopic effect (smaller red shift by 5 cm^{-1}). The predicted effect of deuteration on the shift of the ν(C≡O) band is very small (0.3 cm^{-1}) so that it gives no indication about the complex geometry. We did not find strong experimental indications in the ν(OH) region of complexes III and IV. In the ν(C≡O) region, the bands observed at $\sim$2140 cm^{-1} may originate from the CO dimer isolated in solid Ar.[38,39] In the present experiments, the CO dimers can be formed upon photolysis of either methanol or ketene (see Figure 4). The possibility of ternary complexes involving CO, formaldehyde, and molecular hydrogen producing bands near the free monomer band cannot be excluded.

Upon annealing the matrix at 25 K after photolysis of CH$_3$-COOH, the ν(OH) band (3649.6 cm^{-1}) practically disappears and three new bands appear at 3647.4, 3646.5, and 3645.3 cm^{-1}. A similar intensity reorganization takes place for the ν(C≡O) bands assigned to complex I: the envelope of bands at higher frequency decreases and a new set of bands appear shifted by $\sim$4 cm^{-1} from the decreasing bands (see Figure 7). The observed intensity reorganization is not consistent with conversion to a different complex geometry. In the present case, where only the most stable complex structure is observed upon photolysis, annealing the matrix at 25 K is not expected to decrease its concentration. When photolysis produces a distribution of conformers that is not in thermal equilibrium,[47] annealing the matrix should lead to conversion of the less stable complexes into the lower energy forms. Instead we observed the decrease of bands assigned to the most stable complex. This makes us suggest that the observed modifications are caused by thermal relaxation of the matrix local surrounding, allowing a more
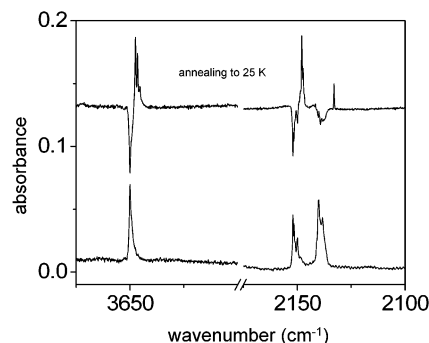
Figure 7. Thermally induced changes on the methanol (ν(OH) mode) and CO bands upon annealing at 25 K. The lower trace shows the spectrum collected after photolysis of acetic acid in solid Ar at 8 K. The upper trace is the difference spectra showing the effect of annealing at 25 K.

suitable orientation of the complex within the cage, in other words, conversion of the matrix sites. The intensity ratio of the increasing and decreasing bands upon annealing is $\sim$1, which supports the fact that the same complex structures produces both sets of bands by taking into account that the ν(OH) absolute intensity is very sensitive to the complex geometry. In fact, the calculated ν(OH) intensities have a ratio of 5:3:1:1 between complexes I:II:III:IV.

There is also a broad feature centered at $\sim$2140 cm^{-1} whose intensity decreases upon annealing to 25 K whereas a new band appears at 2133 cm^{-1}. It is not clear if these bands are related to each other, and the origin of the new narrow band remains unknown. In fact, interpretation of the spectral changes upon annealing are complicated by the fact that there is a small amount of hydrogen atoms that escape the cage during photolysis and can be thermally mobilized. This is a known phenomenon occurring during annealing of a matrix where a molecular species containing hydrogen was photolyzed.[29,57,58] A strong support for mobility of thermally activated hydrogen atoms is the appearance of the band at 1862.4 cm^{-1}, which is in good agreement with the very strong band observed for the free HCO radical in Ar matrixes (1863 cm^{-1}).[59] In the present experimental conditions, the H atom mobility is most probably a local process rather than a global process.

Photolysis Branching Ratios. After identification of the acetic acid photolysis products we can estimate the branching ratios for the proposed photolysis channels. The lack of information on the formation yield of the transient radicals prevents us from clarifying the source of the CO complexes giving bands at $\sim$2140 cm^{-1}. Nevertheless, using the formaldehyde bands we can estimate the percentage of CO molecules involved in ternary complexes with formaldehyde and molecular hydrogen. The ν(C≡O) mode of ketene absorbs at 2140 cm^{-1} in solid Ar, but the relative amount of ketene formed is very small and we neglected its contribution to the envelope of bands around 2140 cm^{-1}. The integrated intensities of the photolysis products, normalized by their intrinsic intensity (calculated or experimental), were used to estimate the proportion of the photolysis channels. The bands at 2150 cm^{-1} were used for complex I between methanol and CO. We chose the CO band (instead of νOH of methanol) because computationally its intrinsic intensity is practically unchanged upon complexation with methanol. The carbon dioxide bands at $\sim$2340 cm^{-1} were used to estimate the importance of the C−C cleavage channel.

As a result, 29% of the acetic acid molecules yield methanol plus carbon monoxide complexes, 15% yield carbon monoxide complexed with formaldehyde and molecular hydrogen, 39%

yield quaternary complexes of two carbon monoxide molecules and two hydrogen molecules and, finally, 17% dissociate to carbon dioxide and methane. Even if we assumed that the absorption of ketene contributes to a half of the intensity of the envelope of bands at 2140 cm^{-1} (which is definitely an overestimate), the percentage of ketene formed upon 193 nm irradiation of acetic acid would be small ($\sim$5%). In this case we would obtain 37%, 17%, 20%, and 21% for the channels connected with CO + CH$_3$OH (complex I), CO + CH$_2$=O + H$_2$ (ternary complex), 2CO + 2H$_2$ (quaternary complex), and CO$_2$ + CH$_4$ complexes, respectively.

The distribution of photodecomposition products is in agreement with the fact that the C—C cleavage, generating carbon dioxide and methane, occurs only on the T$_1$ surface due to energetic restrictions.[17] On the other hand, C—O cleavage occurs both on the S$_1$ and T$_1$ surfaces, meaning that it has a higher probability than the C—C cleavage. Although the intersystem crossing from S$_1$ to T$_1$ is a spin forbidden process, it was concluded that structural similarities between the crossing point of these two surfaces and the S$_1$ minimum indicate that this process can happen to a noticeable extent.[17]

Photolysis of perdeuterated acetic acid shows somewhat different branching ratios when compared with CH$_3$COOH. In the case of CD$_3$COOD, we can evaluate directly the amount of ketene formed from its ν(C=O) band at 2112 cm^{-1}. The estimated percentage of the different products are 45:5:33:16:1 for channels connected with CO + CH$_3$OH:CO + CH$_2$=O + H$_2$:2CO + 2H$_2$:CO$_2$ + CH$_4$:CD$_2$=C=O + H$_2$O. Compared with the photodissociation of CH$_3$COOH, these numbers indicate a considerable difference in the efficiency of the channels leading to formation of CO, formaldehyde, and molecular hydrogen. This is evidenced by the difference in the relative intensity of the CO bands at 2140 and 2150 cm^{-1} upon photolysis of both isotopologues (Figure 5). The deuteration-induced changes in the branching ratios can be caused by isotopic effects on the processes in the scheme presented in Figure 4; however, it is difficult to specify them. For instance, these can include isotope effects of the absorption cross-section of ketene, formaldehyde, methane, methanol, and water at 193 nm.

Conclusions

The results of this work can be separated into four parts:

1. We have analyzed the vibrational spectroscopy of *cis*-acetic acid isolated in solid Ar, which was produced using vibrational excitation of the trans form. The vibrational assignment for various isotopologues was given for the cis form, and some bands were reassigned for the trans form (see Tables 1 and 2).

2. The perdeuterated isotopologue was used to test the conformational selectivity of the solid-state photolysis (193 nm) of acetic acid. No conformational dependence of the acetic acid photodissociation was found. This was explained in terms of decomposition on the excited-state surfaces leading primarily to unselective radical formation.

3. Upon 193 nm irradiation, acetic acid isolated in an Ar matrix decomposes permanently into a number of molecular complexes (see Figure 4 and Table 3). The photodecomposition dynamics for the isolated molecule is complicated, and not all channels are fully understood at the moment. It involves reaction of the radicals formed as primary products and further photodissociation of those secondary products. The major photolysis products are methanol complexed with carbon monoxide, the quaternary complex involving two carbon monoxide molecules and two hydrogen molecules, ternary complexes between carbon monoxide, formaldehyde, and probably molecular hydrogen, and

carbon monoxide complexed with methane. Ketene, which is the main product of thermal decomposition of acetic acid, was detected only in small amounts ($\leq$5%) upon solid-state photolysis of acetic acid, and it is further photolyzed by 193 nm radiation, which makes estimation of its production conditional. In fact, apart from methane and carbon dioxide, all the molecular products observed could be explained in terms of photochemistry of the ketene-water complex.

4. The 1:1 complex between methanol and carbon monoxide was studied on the basis of ab initio calculations. We observed the most stable form of the complex, described by a planar structure with the OH···CO hydrogen bond. Upon annealing at 25 K, the complex structure undergoes small modifications, which are explained in terms of thermal reorganization of the local matrix morphology.

Supporting Information Available: Frequencies and intensities for CH$_3$COOD and CD$_3$COOH. This material is available free of charge via the Internet at http://pubs.acs.org.

References and Notes

(1) Senent, M. L. *Mol. Phys.* **2001**, *99*, 1311.

(2) Haurie, M.; Novak, A. *J. Chim. Phys.* **1965**, *62*, 137.

(3) Wilmshurst, J. K. *J. Chem. Phys.* **1956**, *6*, 1171.

(4) Weltner, W. *J. Am. Chem. Soc.* **1955**, *77*, 3941.

(5) Berney, C. V.; Redington, R. L.; Lin, K. C. *J. Chem. Phys.* **1970**, *53*, 1713.

(6) Burneau, A.; Génin, F.; Quilès, F. *Phys. Chem. Chem. Phys.* **2000**, *2*, 5020.

(7) Nielsen, O. F.; Lund, P.-A. *J. Chem. Phys.* **1983**, *78*, 652.

(8) Johnson, M. R.; Neumann, M.; Nicolai, B.; Smith, P.; Kearly, G. J. *Chem. Phys.* **1997**, *215*, 343.

(9) Kosugi, K.; Makabayashy, T.; Nishi, N. *Chem. Phys. Lett.* **1998**, *291*, 25.

(10) Grenie, Y.; Cornut, J.-C.; Lassegues, J.-C. *J. Chem. Phys.* **1971**, *55*, 5844.

(11) Maçôas, E. M. S.; Khriachtchev, L.; Pettersson, M.; Fausto, R.; Räsänen, M. *J. Am. Chem. Soc.* **2003**, *125*, 16188.

(12) Khriachtchev, L.; Lundell, J.; Isoniemi, E.; Räsänen, M. *J. Chem. Phys.* **2000**, *113*, 4265.

(13) Maçôas, E. M. S.; Lundell, J.; Pettersson, M.; Khriachtchev, L.; Fausto, R.; Räsänen, M. *J. Mol. Spectrosc.* **2003**, *219*, 70.

(14) Pettersson, M.; Lundell, J.; Khriachtchev, L.; Räsänen, M. *J. Am. Chem. Soc.* **1997**, *119*, 11715.

(15) Khriachtchev, L.; Maçôas, E. M. S.; Pettersson, M.; Räsänen, M. *J. Am. Chem. Soc.* **2002**, *124*, 10994.

(16) Goez, M. *Angew. Chem., Int. Ed.* **2003**, *42*, 2336.

(17) Fang, W.-H.; Liu, R.-Z.; Zheng, X.; Phillips, D. L. *J. Org. Chem.* **2002**, *67*, 8407.

(18) Moreira, I. P. R. *J. Mol. Struct. (THEOCHEM)* **1999**, *466*, 119.

(19) Butkovskaya, N. I.; Manke, G. II; Setser, D. W. *J. Phys. Chem.* **1995**, *99*, 11115.

(20) Longfellow, C. A.; Lee, Y. T. *J. Phys. Chem.* **1995**, *99*, 15532.

(21) Owrutsky, J. C.; Baronavski, A. P. *J. Chem. Phys.* **1999**, *111*, 7329.

(22) Hunnicutt, S. S.; Waits, L. D.; Guest, J. A. *J. Phys. Chem.* **1991**, *95*, 562.

(23) Hunnicutt, S. S.; Waits, L. D.; Guest, J. A. *J. Phys. Chem.* **1989**, *93*, 5188.

(24) Peterman, D. R.; Daniel, R. G.; Horwitz, R. J.; Guest, J. A. *Chem. Phys. Lett.* **1995**, *236*, 564.

(25) Pettersson, M.; Khriachtchev, L.; Jolkkonen, S.; Räsänen, M. *J. Phys. Chem. A* **1999**, *103*, 9154.

(26) Bondybey, V. E.; Brus, L. E. *J. Chem. Phys.* **1975**, *62*, 620.

(27) Schriever, R.; Chergui, M.; Schwentner, N. *J. Phys. Chem.* **1991**, *91*, 6124.

(28) Gödderz, K. H.; Schwentner, N.; Chergui, M. *J. Chem. Phys.* **1996**, *105*, 451.

(29) Bondybey, V. E.; Räsänen, M.; Lammers, A. *Annu. Rep. Prog. Chem. C* **1999**, *95*, 331.

(30) Frisch, M. J.; Trucks, G. W.; Schlegel, H. B.; Scuseria, G. E.; Robb, M. A.; Cheeseman, J. R.; Zakrzewski, V. G.; Montgomery, J. A.; Stratmann, R. E.; Burant, J. C.; Dapprich, S.; Millam, J. M.; Daniels, A. D.; Kudin, K. N.; Strain, M. C.; Farkas, O.; Tomasi, J.; Barone, V.; Cossi, M.; Cammi, M.; Mennucci, B.; Pomelli, C.; Adamo, C.; Clifford, S.; Ochterski, J.; Petersson, G. A.; Ayala, P. Y.; Cui, Q.; Morokuma, K.; Malick, D. K.; Rabuck, A. D.; Raghavachari, K.; Foresman, J. B.; Cioslowski, J.; Ortiz, J. V.; Baboul, A. G.; Stefanov, B. B.; Liu, G.; Liashenko, A.; Piskorz, P.; Komaromi, I.; Gomperts, R.; Martin, R. L.; Fox, D. J.; Keith, T.; Al-Laham, M. A.; Peng, C. Y.; Nanayakkara, A.; Gonzalez, C.; Challacombe, M.; Gill, P. M. W.; Johnson, B. G.; Chen, W.; Wong, M. W.; Andres, J. L.; Head-Gordon, M.; Replogle, E. S.; Pople, J. A. *Gaussian 98*, revision A.9; Gaussian, Inc.: Pittsburgh, PA, 1998.

(31) van Duijneveldt, F. B.; van Duijneveldt-van de Rijdt, J. G. C. M.; van Lenthe, J. H. *Chem. Rev.* **1994**, *94*, 1873.

(32) Maçôas, E. M. S.; Khriachtchev, L.; Pettersson, M.; Lundell, J.; Fausto, R.; Räsänen, M. *Vibr. Spectrosc.* **2004**, *34*, 73.

(33) He, H.-Y.; Fang, W.-H. *J. Am. Chem. Soc.* **2003**, *125*, 16139.

(34) Su, H.; He, Y.; Kong, F. *J. Chem. Phys.* **2000**, *113*, 1891.

(35) Naik, P. D.; Upadhyaya, H. P.; Kumar, A.; Sapre, A. V.; Mittal, J. P. *Chem. Phys. Lett.* **2001**, *340*, 116.

(36) Ausloos, P.; Steacie, E. W. R. *Can. J. Chem.* **1955**, *33*, 1530.

(37) Barnes, A. J.; Hallam, H. E. *Trans. Faraday Soc.* **1970**, *66*, 1920.

(38) Dubost, H. *Chem. Phys.* **1976**, *12*, 139.

(39) Abe, H.; Takeo, H.; Yamada, K. M. T. *Chem. Phys. Lett.* **1999**, *311*, 153.

(40) Irvine, M. J.; Mathieson, J. G.; Pullin, A. D. E. *Aust. J. Chem.* **1982**, *35*, 1971.

(41) Khoshkhoo, H.; Nixon, E. *Spectrochim. Acta A* **1973**, *29*, 603.

(42) Romano, R. M.; Védova, C. O. D.; Downs, A. J. *J. Phys. Chem. A* **2002**, *106*, 7235.

(43) Glass, G. P.; Kumaran, S. S.; Michael, J. V. *J. Phys. Chem.* **2000**, *104*, 8360.

(44) Schatte, G.; Willner, H.; Hoge, D.; Knözinger, E.; Schrems, O. *J. Phys. Chem.* **1989**, *93*, 6025.

(45) Lundell, J.; Räsänen, M. *J. Phys. Chem.* **1993**, *97*, 9657.

(46) Lundell, J.; Räsänen, M. *J. Phys. Chem.* **1995**, *99*, 14301.

(47) Heikkilä, A.; Pettersson, M.; Lundell, J.; Khriachtchev, L.; Räsänen, M. *J. Phys. Chem. A* **1999**, *103*, 2945.

(48) Khriachtchev, L.; Pettersson, M.; Tuominen, S.; Räsänen, M. *J. Chem. Phys.* **1997**, *107*, 7252.

(49) Breda, S.; Lapinski, L.; Reva, I.; Fausto, R. *J. Photochem. Photobiol. A.; Chem.* **2004**, *162*, 139.

(50) Jiang, G. J.; Person, W. B.; Brown, K. G. *J. Chem. Phys.* **1975**, *62*, 1201.

(51) Stanton, J. F.; Watts, J. D.; Bartlett, R. J. *J. Chem. Phys.* **1991**, *94*, 404.

(52) Cabana, A.; Savitsky, G. B.; Hornig, D. F. *J. Chem. Phys.* **1963**, *39*, 2942.

(53) Galabov, B.; Yamaguchi, Y.; Remington, R. B.; Shaefer, H. F., III. *J. Phys. Chem. A* **2002**, *106*, 819.

(54) Wen, Y.; Segall, J.; Dulligan, M.; Witting, C. *J. Chem. Phys.* **1994**, *101*, 5665.

(55) Murto, J.; Ovaska, M. *Spectrochim. Acta A* **1983**, *39*, 149.

(56) Latajka, Z.; Ratajczak, H.; Murto, J.; Orville-Thomas, W. J. *J. Mol. Struct.* **1989**, *194*, 45.

(57) Apkarian, V. A.; Schwentner, N. *Chem. Rev.* **1999**, *99*, 1481.

(58) Khriachtchev, L.; Pettersson, M.; Runeberg, N.; Lundell, J.; Räsänen, M. *Nature* **2000**, *406*, 874.

(59) Milligan, D. E.; Jacox, M. E. *J. Chem. Phys.* **1969**, *51*, 277.